

Knowledge Enhanced Conditional Imputation for Healthcare Time-series

Linglong Qian, Joseph Arul Raj, Hugh Logan-Ellis, Ao Zhang, Yuezhou Zhang, Tao Wang, Richard JB Dobson, Zina Ibrahim,

Abstract—We introduce the Conditional Self-Attention Imputation (CSAI), a novel recurrent neural network architecture designed to address the challenges of complex missing data patterns in multivariate time series derived from hospital electronic health records (EHRs). CSAI extends the current state-of-the-art neural network-based imputation methods by introducing key modifications specifically adapted to EHR data characteristics, namely: a) an attention-based hidden state initialisation technique to capture both long- and short-range temporal dependencies prevalent in EHRs, b) a domain-informed temporal decay mechanism to adjust the imputation process to clinical data recording patterns, and c) a non-uniform masking strategy that models non-random missingness by calibrating weights according to both temporal and cross-sectional data characteristics. Comprehensive evaluation across four EHR benchmark datasets demonstrate CSAI’s effectiveness compared to state-of-the-art neural architectures in data restoration and downstream predictive tasks. Additionally, CSAI is integrated within PyPOTS, an open-source Python toolbox designed for machine learning tasks on partially observed time series. This work significantly advances the state of neural network imputation applied to EHRs by more closely aligning algorithmic imputation with clinical realities.

I. INTRODUCTION

Multivariate time series obtained from electronic health records (EHR) play a crucial role in predictive healthcare analytics to derive patient-specific insight [1], [2], [3]. However, EHR time series are characterised by their complexity, and designing successful downstream predictive models requires addressing the abundance of missingness within correlated variables recorded over time. EHR missingness is a direct consequence of clinical and administrative workflows, which inherently lead to variations in the frequency and timing of documenting vital signs, laboratory tests, and other healthcare measures. For example, heart rate is routinely monitored, while data on white blood cell counts are ordered in specific clinical scenarios, such as suspected infection. Furthermore, the structure of EHR data gives rise to numerous correlations between the feature values and their missingness patterns over time. For example, because hypertension is a known cause of kidney disease, not only are high blood pressure measurements expected along with abnormal creatinine levels, but EHR datasets generally show high correlations between the recording patterns of blood pressure and urine creatinine

levels [4]. These inherent irregularities render more than 50% of EHR data missing not at random [5], with significant variations in missingness patterns between tasks and datasets [5]. These challenges create a complex landscape for imputation algorithms [6], [7], [8], [9], [10], [11], [12] and highlight the importance of domain knowledge in improving modelling accuracy.

Recent advances in deep learning have shown significant potential in addressing the complexities of EHR missingness. In particular, models based on recurrent neural networks (RNNs), such as GRU-D [13], BRITS [14], and M-RNN [15], have proven effective in capturing the temporal and cross-sectional dependencies embedded within EHR data. Among these, BRITS has shown superior performance in datasets of varying characteristics [16], [17]. BRITS uses bi-directional RNN dynamics and treats missing data as variables of the bidirectional RNN graph, subsequently involving them in the backpropagation process.

Despite advances, none of the existing models, including BRITS, account for domain-imposed disparities in feature-recording patterns, which can have critical implications on imputation accuracy. We show that incorporating a domain-informed strategy to capture data recording patterns is particularly suited for our domain. In addition, the temporal correlations in the EHR data can span both short- and long-term intervals. For example, while monitoring diabetic patients, both short-term glucose fluctuations and long-term HbA1c levels must be accurately modelled, while cardiovascular risk assessment requires careful cross-sectional examination of biomarkers like cholesterol, glucose, and blood pressure. Although RNNs excel at capturing short-term temporal dependencies in a time series, they are less capable of capturing long-range correlations over time [8]. Finally, all current models rely on random masking as a pre-processing step to generate ground truths for evaluation purposes. This involves designating a randomly selected subset of complete values as missing, primarily creating missing completely at random (MCAR) scenarios and drastically oversimplifying the temporal and cross-sectional dependencies in real EHR time series.

To address these issues, we developed CSAI, a bi-directional RNN using BRITS as a backbone to support a transformer-based attention mechanism for hidden state initialisation and propagation. CSAI extends BRITS to better suit the characteristics of EHR data through the following contributions:

- 1) Improved initialisation of hidden states to more effectively model temporal dynamics between data points.

L. Qian, J. Arul Raj, H. Logan-Ellis, Y. Zhang, T. Wang, R. Dobson and Z. Ibrahim are with the Department of Biostatistics and Health Informatics, King’s College London, London UK

A. Zhang is with the University of Oxford and the The Francis Crick Institute, London UK

Manuscript received November 4, 2024.

Our conditional hidden-state initialisation leverages self-attention to account for long-term dynamics, complementing the short-term dependencies already captured by the RNN and propagating them through the hidden states, thereby improving overall performance.

- 2) We present a domain-informed *temporal decay* function that determines the likelihood of missing values being linked to past observations based on clinical recording patterns derived from the dataset. The decay factor of a feature is used to adjust its associated attention mechanism, enabling a more fine-grained, feature-specific representation of temporal relationships within the data.
- 3) CSAI is integrated with a non-uniform masking strategy to selectively mask data in a way that reflects the naturally structured patterns of interdependencies within the dataset across time and features.

The missing data patterns in the EHR convey clinically relevant information about the variables used in subsequent tasks. Aligning the imputation process with these characteristics can significantly impact the quality of downstream predictive models. CSAI’s contributions better capture domain-specific patterns in EHR data during imputation, leading to improved performance in tasks such as patient-specific prognosis and decision-making.

II. RELATED WORK

The ability of RNNs to capture temporal evolution has made them an attractive choice for time-series imputation. The GRU-D model [13] introduced the use of temporal decay to recurrent imputation models, whereby the influence of past recordings on missing data decreases over time, with features imputed closer to default values if their last observation occurred a long time ago. Using this concept, GRU-D estimates missing values through a combination of the last recorded value and the global mean within a recurrent architecture. Although this approach alone has shown impressive performance in certain healthcare datasets, its effectiveness has not generalised in others [14], particularly with respect to accounting for discrepancies in vital signs recording frequencies and laboratory tests.

Several extensions of GRU-D exist. M-RNN [15] and BRITS [14] use bi-directional RNNs to capture temporal dynamics in both forward and backward directions, improving imputation accuracy. Both M-RNN and BRITS combine RNNs with a feed-forward component to capture additional correlations across features. However, M-RNN treats imputed values as fixed constants while BRITS treats missing values as variables, updating them through backpropagation. Using this strategy, missing values accumulate gradients in both forward and backward directions with consistency constraints, increasing the accuracy of estimated values. BRITS has demonstrated superior performance across various domains [16], [18].

Transformers have shown strong performance in capturing long-term dependencies through their self-attention mechanism [19] and have been used to model missingness at random in SAITS [20]. However, Transformers face challenges in capturing short-term dynamics in time series data and their effectiveness in handling fine-grained temporal details and

complex missing patterns remains debatable [19]. Models like NRTSI [21], though designed to handle these issues, struggle with computational complexity [20].

Some imputation efforts prioritise the ability to quantify one’s confidence in the resulting imputation, introducing stochasticity into their architectures. This includes RNN-based models such as GRU-U [22], variational autoencoders such as V-RIN [23], generative adversarial networks such as E^2 GAN [24] and diffusion models as in CSDI [25]. Apart from CSDI, all these approaches require additional stochastic modules added to the imputing network, resulting in unstable training due to increased coupling, and ultimately leading to less accurate imputation in comparative studies [26]. Although CSDI [25] successfully exploits the correlations between observed values to measure stochasticity, it suffers from data leakage as indicated in its repository.

CSAI aims to build on the current state of neural network imputation by addressing unsolved challenges. By encoding transformer-based self-attention to a bi-directional RNN architecture, CSAI captures long-term dependencies which may be missed by BRITS and similar RNN-based models [14]. Furthermore, introducing the domain-informed temporal decay function refines the imputation process beyond standard decay techniques [13]. Finally, integrating CSAI with a non-uniform masking strategy specifically targets the complex temporal and cross-sectional relationships in EHRs.

III. TERMINOLOGY AND BACKGROUND

A. Incomplete Multivariate Time-series Representation

For a temporal observation over T discrete time steps, we represent a multivariate time series as a matrix $\mathbf{X} \in \mathbb{R}^{T \times D}$. $\mathbf{X} = \{\mathbf{x}_1, \mathbf{x}_2, \dots, \mathbf{x}_T\}$ is composed of T observations, each denoted by a vector $\mathbf{x}_t \in \mathbb{R}^{1 \times D}$ of D features observed at timestamp s_t .

Information related to missing values is encapsulated within two derived matrices (see Fig.1). The mask matrix $\mathbf{M} \in \mathbb{R}^{T \times D}$ indicates whether each element of \mathbf{X} is observed or missing:

$$m_t^d = \begin{cases} 0, & \text{if } x_t^d \text{ is missing} \\ 1, & \text{otherwise} \end{cases} \quad (1)$$

Furthermore, given that the time elapsed between consecutive observations can vary, we denote the time gaps at each time step by an additional component δ_t^d . $\delta_t^d \in \mathbb{R}^{T \times D}$ encodes the time gap between two successive observed values for each feature d , providing an additional indicator of temporal context to the dataset.

$$\delta_t^d = \begin{cases} s_t - s_{t-1} + \delta_{t-1}^d & \text{if } t > 1, m_t^d = 0 \\ s_t - s_{t-1} & \text{if } t > 1, m_t^d = 1 \\ 0 & \text{if } t = 1 \end{cases} \quad (2)$$

B. Overview of the BRITS Backbone

BRITS exploits cross-sectional and temporal correlations in multivariate time series through two dedicated components, a fully connected regression module and a recurrent module,

Time series X					Mask					Time gap					
5	/	/	8	9	1	0	0	1	1	0	4	5	7	2	$d = 1$
7	/	/	/	9	1	0	0	0	1	0	4	5	7	9	$d = 2$
2	4	1	6	/	1	1	1	1	0	0	4	1	2	4	$d = 3$
x_1	x_2	x_3	x_4	x_5	m_1	m_2	m_3	m_4	m_5	δ_1	δ_2	δ_3	δ_4	δ_5	

Fig. 1. An example of multivariate time-series. Observations x_{1-5} in time-stamps $s_{1-5} = 0, 4, 5, 7, 9$. Feature d_2 was missing during s_{2-4} , the last observation took place at s_1 . Hence, $\delta_5^2 = t_5 - t_1 = 9 - 0 = 9$.

respectively. The BRITS architecture accepts a time series \mathbf{X} , such that missing values within an observation $x_t \in \mathbf{X}$ are managed via a corresponding masking vector m_t and a time gap vector δ_t as shown at the bottom of Fig.2.

Because an observation x_t may contain missing values, it cannot be directly ingested by the two BRITS components. Instead, BRITS uses the notion of *decay* to derive estimates for missing cells. Temporal decay dictates that the strengths of the correlations are inversely related to the time-gap δ_t and is formalised by the decay factor $\gamma_t \in (0, 1]$, Eq.(4). In the equation, \mathbf{W}_γ and \mathbf{b}_γ are parameters. The calculated decay factor γ_t for the hidden state is then used to transform h_{t-1} to the *decayed* hidden state, \hat{h}_{t-1} as in Eq.(5). BRITS uses the decayed hidden state to find the historical estimation \hat{x}_t , of x_t as in Eq.(6). Using masking vector m_t obtained from \mathbf{M} , \hat{x}_t is then used to replace the missing values of x_t , yielding the *complement vector* x_t^h , which embeds temporal missingness patterns to be fed into subsequent BRITS components, Eq.(7).

$$h_0 = 0 \quad (3)$$

$$\gamma_{th} = \exp(-\max(0, \mathbf{W}_\gamma \delta_t + \mathbf{b}_\gamma)) \quad (4)$$

$$\hat{h}_{t-1} = h_{t-1} \odot \gamma_t \quad (5)$$

$$z\hat{x}_t = \mathbf{W}_x \hat{h}_{t-1} + \mathbf{b}_x \quad (6)$$

$$x_t^h = m_t \odot x_t + (1 - m_t) \odot \hat{x}_t \quad (7)$$

BRITS explores cross-sectional correlations within a single observation through a fully connected layer, generating x_t^f , a feature-wise approximation of missing values, Eq.(8). The concept of decay extends to the feature space, resulting in a learnable factor β_t , taking into account the temporal decay and the masking vector, Eq.(9)-(10). This integration produces the imputed matrix x_t^c , effectively combining observed and imputed data (Eq.(11)-(12)).

$$x_t^f = \mathbf{W}_z x_t^h + \mathbf{b}_z \quad (8)$$

$$\gamma_{tf} = \exp(-\max(0, \mathbf{W}_{\gamma f} \delta_t + \mathbf{b}_{\gamma f})) \quad (9)$$

$$\hat{\beta}_t = \sigma(\mathbf{W}_\beta [\gamma_{tf} \odot m_t] + \mathbf{b}_\beta) \quad (10)$$

$$\hat{x}_t^c = \beta_t \odot x_t^f + (1 - \beta_t) \odot x_t^h \quad (11)$$

$$x_t^c = m_t \odot x_t + (1 - m_t) \odot \hat{x}_t^c \quad (12)$$

$$h_t = \sigma(\mathbf{W}_t \hat{h}_{t-1} + \mathbf{U}_h [x_t^c \odot m_t] + \mathbf{b}_h) \quad (13)$$

The final step of BRITS updates the hidden state via its RNN component, leveraging various indicators to learn functions of past observations, Eq.(13). Bidirectional recurrent dynamics is used to address slow convergence by using information in the backward direction. The entire process is shown within the BRITS bidirectional architecture in Fig.2

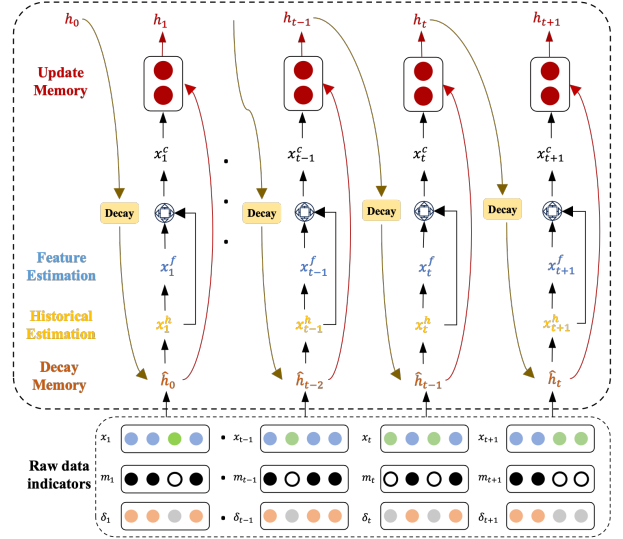


Fig. 2. The BRITS backbone process

IV. METHODOLOGY

In this section, we describe the modifications proposed to the BRITS architecture to incorporate a) a domain-informed temporal decay functionality, b) the ability to capture long-range correlations via a transformer-based conditional hidden state initialisation, and c) a novel non-uniform masking strategy to explicitly model non-random EHR missingness. The section concludes with the resulting learning framework of CSAI.

A. EHR-Tailored BRITS Adaptations

Domain-informed Temporal Decay: The BRITS decay function Eq.(4) is strictly dependent on temporal proximity, dynamically adjusting the contribution of a past observation to a missing value based on the length of the time gap between the two. Although this decay mechanism effectively captures the intuition that more recent observations carry greater diagnostic value, it overlooks domain-specific discrepancies, where different features follow distinct recording frequencies due to clinical practices. This can be illustrated in the example below.

Example 1. Let features f_1 and f_2 represent heart rate (HR) and systolic blood pressure (SBP), respectively. As a vital sign indicative of a patient's state, HR is typically monitored at more frequent intervals compared to SBP. BRITS is presented with an observation x_t where both HR and SBP values are missing. The time gap vector δ_t shows $\delta_t^{f_1} = 2$ (indicating that the last HR recording occurred 2 time units ago) and $\delta_t^{f_2} = 7$ (indicating that the last SBP recording occurred 7 time units ago).

According to the principle of temporal decay, BRITS would apply a stronger influence from the more recent HR observation compared to the older SBP observation, despite the fact that SBP is typically recorded less frequently and still carries significant diagnostic importance. Consequently, BRITS would incorrectly assign less weight to the last SBP observation compared to HR, overlooking the domain-specific recording

patterns, where the last recording of SBP, despite a longer time gap, remains a critical input for imputation.

Our proposed new decay mechanism prioritises recent observations while accounting for the natural variability in healthcare data collection. In addition to using the observed time gap δ_t^d , we modify the decay function to incorporate the expected time gap τ between two recordings of a given feature. The expected time gap τ_d for a feature is computed as the median of the time intervals between successive recordings of feature d in the dataset. This adjustment allows the decay function to adapt to the recording patterns of different clinical features, ensuring that features like SBP, which are recorded less frequently, still carry appropriate weight during imputation.

The new decay factor γ_t^d for a feature d at time t is computed as:

$$\gamma_t^d = \exp(-\max(0, W_\gamma(\delta_t^d - \tau_d) + b_\gamma)) \quad (14)$$

Where:

- δ_t^d is the time gap since the last observation of feature d ,
- τ_d is the median time gap for feature d ,
- W_γ and b_γ are learnable parameters.

This formulation ensures that the decay factor peaks when the time gap δ_t^d closely matches the expected time gap τ_d , and declines as the difference between δ_t^d and τ_d increases. Thus, observations that fall within their expected time gap contribute more strongly to the imputation process, while those that lie far outside the expected gap are down-weighted as illustrated in the example below.

Example 2. For the same features f_1 and f_2 , examining the dataset reveals that the median time gaps for the two features are $\tau_1 = 2$ for HR and $\tau_2 = 10$ for SBP. These medians reflect the fact that HR is routinely monitored more frequently than SBP in clinical practice. By leveraging these median time gaps, the model can account for the different recording frequencies. Here, since the last observed values for both HR and SBP fall within their respective median time gaps, the model assigns comparable importance to both past recordings when imputing the missing values. This approach ensures that the less frequently measured SBP, with its median gap of 10, is not unfairly penalised, preserving the clinical relevance of both features.

Attention-based Hidden State Initialisation: The hidden state of the recurrent component of BRITS are not generated through the raw input. Instead, they receive incomplete data with missingness indicators for imputation, i.e. $\hat{\mathbf{h}}$ replaces \mathbf{h} in Eq.(5). However in BRITS, the initial hidden state is initialised to zero as in Eq. 3, which causes the model to rely solely on its internal parameters to estimate initial missing values in Eq. 6, ignoring crucial information from prior observations. This can be particularly problematic in medical data, where early data points are often crucial to understanding patient trends, and failure to incorporate them can lead to inaccurate imputations and the loss of important clinical insights as illustrated by the example below.

Example 3. Consider a patient whose heart rate (HR) and systolic blood pressure (SBP) are being monitored. Over the last few recorded measurements, the patient’s HR has been steadily increasing, indicating a deteriorating condition. However, there is a monitoring gap leading to missing initial values. With the hidden state initialised to zero, BRITS would not only fail to capture the upward trend in HR by disregarding the critical information from later measurements, but could also propagate erroneous assumptions about stability throughout the time series. As the hidden state learns from the imputed values, it would continuously stack these errors, potentially amplifying the misrepresentation of the patient’s condition as stable when in fact urgent intervention is required.

To solve this issue, our approach makes use of the last observed data point and a decay attention mechanism to generate a conditional distribution for the initial hidden state $\mathbf{q}(\mathbf{h}_{\text{init}}|\mathbf{x}_{\text{last_obs}}, \gamma_t^d)$ within the model distribution $\mathbf{p}_\theta(\mathbf{x}_t)$. This strategy is designed to provide a more contextually rich starting point for the model, thus enhancing the effectiveness of subsequent imputations. Instead of applying the decay factor directly to the previous hidden state as done in BRITS (Eqs. (5) and Eq.(10)), we use the decay factor to modulate an attention mechanism to better capture long-range and feature-specific temporal dynamics, discussed below.

First, at each time step s_t , the last observation $\mathbf{x}_{\text{last_obs}} \in \mathbb{R}^{T \times D_{\text{feature}}}$ and the decay factor γ_t^d are projected and encoded to capture their temporal positioning within the sequence:

$$\mathbf{x}'_{\text{last_obs}} = \text{PosEncoder}(\text{InputProj}(\mathbf{x}_{\text{last_obs}})) \quad (15)$$

$$\gamma'_t = \text{PosEncoder}(\text{InputProj}(\gamma_t^d)) \quad (16)$$

Then the transformed input representations are concatenated and fed into a Transformer encoder, which is capable of capturing both long-range dependencies and feature-specific interactions:

$$\mathbf{C}_{\text{in}} = \text{Concat}(\mathbf{x}'_{\text{last_obs}}, \gamma'_t) \quad (17)$$

$$\mathbf{C}_{\text{out}} = \text{LN}(\text{FFN}(\text{LN}(\text{MSA}(\mathbf{C}_{\text{in}})))) \quad (18)$$

The output of the Transformer is then passed through a series of 1D convolutional layers to adjust the dimensions and initialise the hidden state:

$$\mathbf{H}_1 = \text{Conv1D}_1(\mathbf{C}_{\text{out}}\mathbf{W}_1 + \mathbf{b}_1) \quad (19)$$

$$\mathbf{h}_{\text{init}} = \text{Conv1D}_2(\mathbf{H}_1\mathbf{W}_2 + \mathbf{b}_2) \quad (20)$$

where Eq.(19) transforms \mathbf{C}_{out} from $\mathbb{R}^{2L \times d_{\text{model}}}$ to $\mathbb{R}^{2L \times d_{\text{hidden}}}$ and produces \mathbf{H}_1 , Eq.(20) further scales \mathbf{H}_1 to generate the initialised Hidden State \mathbf{h}_{init} . This Transformer-based hidden-state initialisation allows the model to better capture the temporal dynamics and variability in feature-recording patterns, providing a more robust foundation for subsequent imputation steps. The CSAI architecture is shown in Figure 3.

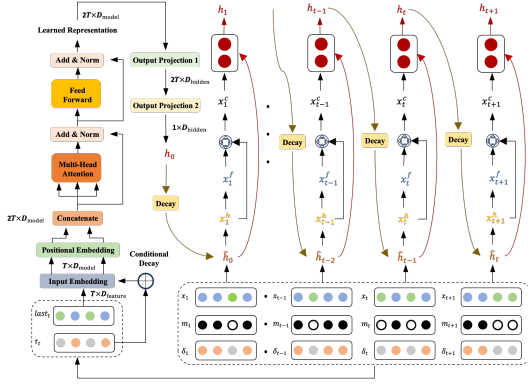


Fig. 3. The CSAI architecture, which equips BRITS with self-attention. CSAI begins with an input embedding layer, followed by positional embedding to capture time dependencies. These embeddings are processed through multi-head attention, normalization, and feed-forward layers. The output is used to initialize hidden states for subsequent recurrent layers, accounting for both temporal dynamics and domain-specific variability in recording patterns.

B. Non-Uniform Masking Strategy

Our non-uniform masking strategy fundamentally diverges from traditional approaches by leveraging the missingness distribution within the dataset. Our strategy is predicated on the principle outlined in the introduction, whereby the probability of missingness in healthcare data is not uniformly distributed across features. Instead, it varies according to healthcare practices and patient conditions. By incorporating this variability into our masking process, we aim to create a more realistic and representative model of the missingness patterns within the dataset.

Our masking algorithm generates masking probabilities using two factors:

- 1) **Missingness Distribution** $P_{\text{dist}}(d)$: This reflects the likelihood of masking a feature based on its missingness patterns across similar or neighboring observations.
- 2) **Adjustment Factor** $R_{\text{factor}}(d)$: A dynamic value that adjusts the masking probability based on how often the feature d is observed. Frequently observed features are masked less to avoid overfitting, while sparsely observed features are masked more to ensure sufficient model learning from limited data points.

For a given feature d , the non-uniform masking probability $P_{\text{nu}}(d)$ is determined as follows:

$$\mathbf{R}_{\text{factor}}(d|U, I) = \mathbf{F}(d, U, I) \quad (21)$$

$$\mathbf{P}_{\text{nu}}(d) = \mathbf{R}_{\text{factor}}(d|U, I) \times \mathbf{P}_{\text{dist}}(d) \quad (22)$$

Where:

- U and I are the pre-defined parameters. U is the masking rate, i.e. the percentage of the ground truths masked during training. I is a weighting parameter.
- $\mathbf{R}_{\text{factor}}(d|U, I)$ is the adjustment factor for feature d , conditioned by U and I .
- $\mathbf{P}_{\text{dist}}(d)$ is d 's missingness probability distribution.

The overall masking proportion is then adjusted to ensure consistency with the uniform masking rate U , while retaining the non-uniform characteristics of the individual features. The

pseudocode for this algorithm is given below, producing a masked matrix \mathbf{X}_M .

Algorithm 1 *non-uniform-mask*

Input: Dataset \mathbf{X} with D features, masking rate U , weighting parameter I

Output: Masked Dataset \mathbf{X}_M

for each feature d in D **do**

$$\mathbf{P}_{\text{dist}}(d) \leftarrow \text{compute}(\mathbf{x}^d)$$

$$\mathbf{R}_{\text{factor}}(d) \leftarrow f(U, I)$$

$$\mathbf{P}_{\text{nu}}(d) \leftarrow \mathbf{R}_{\text{factor}}(d) \times \mathbf{P}_{\text{dist}}(d)$$

end for

$$\mathbf{U} \leftarrow f(\mathbf{P}_{\text{nu}}, \mathbf{X})$$

$$\mathbf{X}_M \leftarrow \mathbf{P}_{\text{nu}} \times \mathbf{X}$$

C. Learning

CSAI is trained in an unsupervised manner by stochastically masking non-missing values using our non-uniform masking strategy and learning to impute them. At evaluation time, the trained RNN can impute both real and simulated missing values. CSAI's training iterates over mini-batches of the input data, where each mini-batch comprises a set of samples with T time steps. Our imputation loss function \mathcal{L}_{imp} maintains the objective of minimising the reconstruction error ℓ_{obs} between the imputed and ground truth vectors \mathbf{x} and $\hat{\mathbf{x}}$, while maintaining consistency loss ℓ_{con} between the forward and backward imputed estimates $\vec{\hat{\mathbf{x}}}$ and $\overleftarrow{\hat{\mathbf{x}}}$ of our bi-directional RNN.

CSAI's training iterates over mini-batches of the input data, where each mini-batch comprises a set of samples with T time steps. Our imputation loss function \mathcal{L}_{imp} maintains the objective of minimising the reconstruction error ℓ_{obs} between the imputed and ground truth vectors \mathbf{x} and $\hat{\mathbf{x}}$, while maintaining consistency loss ℓ_{con} between the forward and backward imputed estimates $\vec{\hat{\mathbf{x}}}$ and $\overleftarrow{\hat{\mathbf{x}}}$ of our bi-directional RNN as follows:

$$\mathcal{L}_{\text{imp}} = \frac{1}{|\mathcal{B}|} \sum_{i \in \mathcal{B}} \sum_{t \in T_i} \lambda \left[\mathbf{M}_{it} \odot \ell_{\text{obs}}(\mathbf{x}_{it}, \hat{\mathbf{x}}_{it}) + (1 - \mathbf{M}_{it}) \odot \ell_{\text{con}}(\vec{\hat{\mathbf{x}}}_{it}, \overleftarrow{\hat{\mathbf{x}}}_{it}) \right] \quad (23)$$

Where \mathcal{B} is the mini-batch size, T is the set of time steps over which the loss function is applied, \mathbf{M} is the masking matrix and λ is a hyperparameter that balances the two loss terms. Both ℓ_{obs} and ℓ_{cons} use the mean absolute error (MAE) to measure the difference between the components of each loss function.

Since CSAI can be used as an end-to-end pipeline to perform imputation and prediction, we further define prediction loss using binary cross-entropy as follows:

$$\mathcal{L}_{\text{pred}} = - \sum_{n=1}^N y^{(n)} \log(\hat{y}^{(n)}) \quad (24)$$

The resulting combined loss is computed as:

$$\mathcal{L}_{\text{combined}} = \alpha\mathcal{L}_{\text{imp}} + \beta\mathcal{L}_{\text{pred}} \quad (25)$$

Where β With α and β are preset parameters representing the weight of the respective loss component on $\mathcal{L}_{\text{combined}}$. Using CSAI solely as imputer is done by setting β to zero. With this loss function, CSAI uses backpropagation in an end-to-end manner to optimise model parameters during training.

V. EXPERIMENTAL EVALUATION

We conducted several experiments to evaluate the proposed methodologies and their impact on CSAI’s performance on widely-used healthcare benchmark datasets. First, we describe the datasets, followed by the experimental design and implementation details, and conclude with the results.

A. Datasets

We used three healthcare benchmarks obtained from three widely used databases. Each of the datasets used has a different data distribution and characteristics as shown in Table I.

1) **eICU**¹ [27] is a multicentre database with anonymised patient records from intensive care units (ICU) obtained from more than 200 hospitals. eICU is publicly available after registration. We followed the only benchmark extract available for eICU [28].

2) **MIMIC-III**² [29] is an extensive, single-hospital database of over 40,000 critical care patients. We used MIMIC-III to increase the heterogeneity of our datasets with different features types and data dimensionality and followed a well-cited benchmark [30] to produce a dataset comprising 59 numerical variables for 21,128 samples.

3) **PhysioNet Challenge 2012 dataset** is a public medical benchmarking dataset provided by [31], containing records of 4000 48-hour hospital stays, allowing unbiased evaluations of different model performances. This benchmark comprises 35 numerical variables for 3,997 samples.

For all data sets, we reproduced the available benchmarking, skipping the steps that remove all-NAN samples to retain the data with its original missingness.

B. Experimental Design

We conducted two sets of experiments to test the methodologies proposed in this work. The first comprises **benchmark comparison experiments** comparing CSAI’s imputation and subsequent classification performance against the current state of the art on two scales:

1) **Experiment I:** compares CSAI with the best-performing RNN models using the three benchmark datasets and three masking ratios (5%, 10% and 20%). Here, CSAI is compared with our backbone bidirectional RNN model BRITS [14], the Gated Recurrent Unit with Decay (GRU-D) [13], the Variational Recurrent Imputation Network (V-RIN) [23], and the Multi-directional Recurrent Neural Network (M-RNN)

model [15]. In this experiment, two tasks were undertaken to ensure a fair comparison: 1) because the original BRITS implementation uses LSTM cells while all other baseline models use GRU cells, we implemented a GRU-based BRITS model to ensure a balanced evaluation across similar architectures, including its output along with the original BRITS (BRITS-GRU in the results), 2) we employed our nonuniform masking algorithm as a pre-processing step for all models to avoid any bias arising from the masking step.

2) **Experiment II:** is a large-scale experimental evaluation with different flavours of neural imputation models using the Physionet dataset with a 10% masking ratio. This experiment was conducted using the PyPOTS library³ [32], an open-source Python toolkit for benchmarking and analysing incomplete multivariate time series. PyPOTS provides access to 29 imputation algorithms, including CSAI and a number of benchmark datasets, including Physionet. In this experiment, CSAI is compared against a broad range of neural network imputation models, such as Transformers, CNNs, GNNs, and diffusion models, as well as RNNs and standard statistical imputation methods. As non-uniform masking is not yet integrated into PyPOTS, we rely on the available masking setup, aiming to evaluate the contribution of CSAI’s temporal decay and attention mechanism on the resulting performance.

The reader should note that although a comparison with generative models through E^2 GAN [33] would have provided valuable insight, particularly given its lack of its quantitative comparison with BRITS, the publicly available implementation of E^2 GAN is incompatible with our current setup and is also not part of PyPOTS.

The second set of experiments are **ablation studies** performed using the public Physionet dataset. First, we establish the effect of non-uniform masking across different data partitions, namely the training, validation, and test sets. The aim is to establish whether this approach actually improves a model’s ability to generalise and handle missing data in a more realistic and robust manner. Finally, we evaluate the effect of the weighting parameter, which controls the degree of emphasis placed on different features in the non-uniform masking strategy. This parameter allows for fine-tuning of the feature representation during model training, directly influencing how the model handles missing data and we evaluate the effect on CSAI’s imputation and classification performance under different weighting parameter values.

C. Experimental Setup

Environment: We trained our models on an HPC node equipped with an NVIDIA A100 40GB GPU, running Ubuntu 20.04.6 LTS (Focal Fossa). The experiments were carried out using Python 3.8.16. For the first set of experiments comparing CSAI with other RNN models, we directly used the source code for BRITS, GRU-D, and MRNN, obtained from their respective repositories, along with CSAI. For the broader set of experiments comparing CSAI with all neural imputation models, we utilised the PyPOTS implementation of all models,

¹<https://physionet.org/content/eicu-crd/2.0/>

²<https://physionet.org/content/mimiciii/1.4/>

³<https://pypots.com/about/>

Dataset	Size	Avg Baseline Missingness	Feature Correlation	(Static; Categorical) Variables
eICU	30,680 x 20	40.53%	0.14	(6; 3)
MIMIC_59	21,128 x 59	61%	0.17	(0;0)
Physionet	3,997 x 35	51%	0.12	(0; 0)

TABLE I

CHARACTERISTICS OF THE FOUR DATASETS: **SIZE** IS DESCRIBED AS NUMBER OF SAMPLES \times NUMBER OF VARIABLES. **AVERAGE BASELINE MISSINGNESS** OF ALL FEATURES. **FEATURE CORRELATION** IS THE AVERAGE FEATURE-WISE PEARSON CORRELATION COEFFICIENT. **(STATIC; CATEGORICAL)** THE NUMBER OF STATIC (AS OPPOSED TO DYNAMIC) AND CATEGORICAL (AS OPPOSED TO NUMERICAL) VARIABLES IN THE DATASET.

running all experiments through the PyPOTS package installed on our HPC node. Full package details can be found in our repository. To help reproduce our Python environment easily, we freeze the development environment with Anaconda and save it into file for reference, which is available in the project’s GitHub repository. To ensure reproducibility of our results, we release all data preprocessing scripts, model implementations, and hyperparameter search configurations.

Dataset Pre-processing and Missingness Patterns Simulation: Each dataset was normalised to zero mean and unit variance. For each of the four datasets, we created three versions by further masking 5%, 10% and 20% cells in addition to the missingness already present in the original datasets. These masked cells have known ground truths and will form the basis of our comparison of imputation performance. To more effectively simulate EHR missingness scenarios, our first set of experiments use our non-uniform masking as a pre-processing step to enable capturing patterns representative of common missingness data mechanisms in EHRs to the masked cells. In our wider experiments using PyPOTs, we used the package’s PyGrinder toolbox⁴, which implements structured missingness patterns that reflect the dynamic nature of time series data [34], [35], [36].

Hyper-parameter Optimisation: The performance of deep-learning models highly depends on the settings of hyper-parameters. To make fair comparisons across imputation methods and draw impartial conclusions, hyper-parameter optimisation is applied to all imputation algorithms using PyPOTs.

Training: Except the PhysioNet dataset which already contains separated time series samples, all other datasets are split into training, validation, and test sets. Randomly, we selected 10% of each dataset for validation and another 10% for testing, training the models on the remaining data. We used the Adam optimiser and set the number of RNN hidden units to 108 for all models. The batch size is 64 for PhysioNet and 128 for the other datasets. A 5-fold cross-validation method was implemented to evaluate the models.

Downstream Task Design: To evaluate the impact of imputation on downstream analysis, we further perform a classification task to predict in-hospital mortality. In the Physionet dataset, each sample has a label indicating whether the patient is deceased in the ICU. For all other datasets, we extracted the results for each patient according to the code provided in the

benchmark. To demonstrate the flexibility of the model and its ability to perform using different classification architectures, we used different methodologies to implement the classifiers in our experiments. In **Experiment I**, classification was performed in an end-to-end manner by adding a classification layer to each architecture, utilising the hidden states from the imputation network to feed into the classification layer. In **Experiment II**, the imputation models were used to generate complete datasets, which were subsequently fed into three different classifiers for comparison: an XGBoost, an RNN and a Transformer classifier.

Evaluation Metrics: To assess imputation performance, we use mean absolute error (MAE) [14] defined as:

$$\text{MAE} = \frac{1}{n} \sum_{i=1}^n |y_i - \hat{y}_i|$$

Where:

- n is the number of data points,
- y_i is the actual value for the i -th data point,
- \hat{y}_i is the predicted value for the i -th data point.

For classification, we use the Area Under the Receiver-Operator Curve (ROC-AUC) to report performance.

D. Experimental Results

Experiment I: Comparison with State-of-the-Art RNN Models on Healthcare Benchmarks: Our evaluation of CSAI against four state-of-the-art RNN imputation models on all three healthcare benchmarks across three masking ratios is shown in Tables II and III. Table II shows the imputation performance, where CSAI consistently outperforms other models in all data sets and masking ratios (5%, 10%, and 20%). The best performance for all models is observed on the eICU and MIMIC_59 datasets, which, despite high missingness rates, offers a large number of samples for training. The Physionet dataset, while having the lowest baseline missingness rate, provides significantly fewer samples compared to the other datasets, limiting model performance across the board. The table also shows that the performance gap between CSAI and other models widens as the masking ratio increases, leading to conditions of high data loss. This is particularly pronounced in the highly-dimensional dataset MIMIC_59 at the 20% missingness ratio. For V-RIN, BRITS, and BRITS_GRU, the MAE is relatively stable across masking ratios but remains consistently higher than CSAI. GRUD and MRNN show

⁴<https://pypots.com/ecosystem/#PyGrinder>

TABLE II

IMPUTATION PERFORMANCE USING 5%, 10%, AND 20% MASKING RATIOS ON THREE DATASETS. THE MODEL WITH THE LOWEST MAE IN EACH SETUP IS HIGHLIGHTED IN BOLD.

	eICU (MAE)			MIMIC_59 (MAE)			PhysioNet (MAE)		
	5%	10%	20%	5%	10%	20%	5%	10%	20%
V-RIN	0.24161 ± 0.015	0.24254 ± 0.013	0.25214 ± 0.019	0.15457 ± 0.007	0.13818 ± 0.017	0.33697 ± 0.010	0.26163 ± 0.015	0.27372 ± 0.010	0.29997 ± 0.018
BRITS	0.16699 ± 0.014	0.17053 ± 0.020	0.17681 ± 0.009	0.15195 ± 0.018	0.14023 ± 0.009	0.34039 ± 0.019	0.25634 ± 0.013	0.26762 ± 0.017	0.28722 ± 0.014
BRITS_GRU	0.17232 ± 0.010	0.17124 ± 0.019	0.17691 ± 0.013	0.14793 ± 0.016	0.14193 ± 0.015	0.34169 ± 0.017	0.25129 ± 0.012	0.26216 ± 0.011	0.28288 ± 0.018
GRUD	0.22274 ± 0.018	0.22560 ± 0.010	0.23098 ± 0.020	0.30447 ± 0.012	0.28704 ± 0.014	0.48670 ± 0.017	0.49406 ± 0.015	0.49779 ± 0.020	0.50952 ± 0.018
MRNN	0.47036 ± 0.015	0.47998 ± 0.017	0.50065 ± 0.020	0.30573 ± 0.013	0.28342 ± 0.012	0.47198 ± 0.015	0.54671 ± 0.013	0.55647 ± 0.014	0.57230 ± 0.017
CSAI	0.15967 ± 0.017	0.16149 ± 0.011	0.16637 ± 0.015	0.13119 ± 0.009	0.11291 ± 0.008	0.30976 ± 0.014	0.24602 ± 0.014	0.25747 ± 0.017	0.27476 ± 0.019

notably higher MAE values, especially at higher masking ratios.

Table III further demonstrates CSAI’s strong classification performance, achieving the highest AUC scores across various masking ratios in the eICU, PhysioNet, and MIMIC_59 datasets. The difference between CSAI’s AUCs and those of other models is highest under the Physionet dataset, which has the smallest number of samples. Across all three datasets, CSAI’s AUC only slightly decreases as the masking ratio increases to 20%. Although a similar stability is observed in BRITS and V-RIN, the AUCs are consistently lower than CSAI’s.

Experiment II: Large-scale Comparison Using PyPOTs:

Table IV shows classification results for 24 neural imputation models and four statistical imputers. This experiment uses the imputed data generated by each model as input to a classifier. We show the results for three classifiers, and XGBoost, RNN and a Transformer classifier. The reader should not that non-uniform masking was not implemented into CSAI here, since it is yet to be integrated into a callable capability in the PyPOTs library and it is therefore not possible to use it with any other imputation models apart from CSAI.

Overall, the XGBoost classifier achieved the best performance, with a mean AUC of 0.823 compared to 0.660 for the RNN classifier and 0.667 for the Transformer. With XGBoost, using CSAI as an imputer produced the best classification performance. Since XGBoost is a non-temporal model, it has clearly benefited from CSAI’s ability to encode sequential dependencies (across features and time) as informative features that complement XGBoost’s strengths in feature-based learning. For both the RNN and Transformer classifiers, diffusion models produced the highest AUCs, largely due to their ability to offer RNN and Transformer imputers the advantage of smoother interpolations that likely enhance feature consistency across time steps, which is crucial for sequential models. Despite this, CSAI ranked highly under these classifiers, producing competitive AUC performance as a lightweight, efficient model that avoids the computational burden of diffusion models.

Ablation Study Figure 4 demonstrates a clear progression in CSAI’s performance as its components are incrementally added. Starting from the baseline, the model’s MAE improves with each addition, highlighting the impact of the domain-informed temporal decay, attention-based initialisation mechanism, and non-uniform masking. The final configuration, with

all components included, achieves the lowest MAE across all three datasets. These results indicate that each component plays a distinct role in enhancing imputation accuracy, with the full model yielding the best performance.

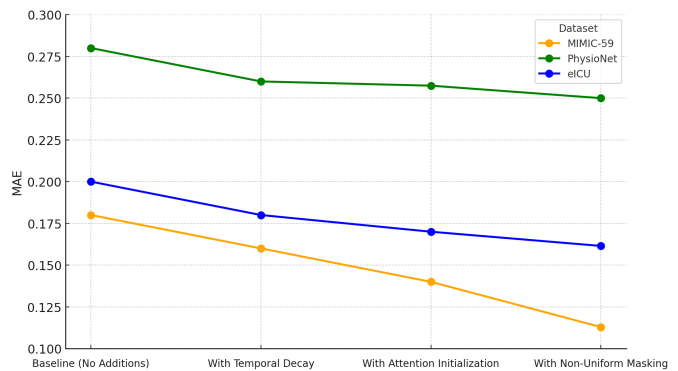


Fig. 4. Visualisation of the incremental increase in imputation performance (decrease in MAE) as the different components of CSAI are incrementally added. The figure shows CSAI’s MAE using the three datasets and 10% masking ratio and the following variations: a) baseline model (i.e. a BRITS architecture), b) adding the temporal decay function, c) adding the attention-base initialisation mechanism, and finally d) using non-uniform masking.

We further evaluate the effect of non-uniform masking on algorithm performance by using the masking strategy on different combinations of the training, validation and test sets and examining the number of training epochs required to achieve the reported performance for each. For objective evaluation of our non-uniform masking strategy, we conducted all experiments using the BRITS and BRITS-GRU baseline models, with the results shown in Table V. These results demonstrate that consistently applying non-uniform masking across all data partitions (training, validation and testing) yields the best performance, suggesting that the masking strategy effectively adjusts the representation of different features to optimally leverage the data distribution, enhancing the model’s ability to handle the inherent heterogeneity of the dataset.

The non-uniform masking probability used by CSAI for each feature is determined the parameters U and I , in addition to the feature’s prior probability as shown in Eq.(21)- (22). We studied the effect of the weighting parameter I on the resulting imputation and classification performance. The findings are shown in Table VI and are further illustrated in Fig.5. An optimal weighting parameter, shown to be around 5, results in the lowest imputation error, suggesting that a balanced

TABLE III

CLASSIFICATION PERFORMANCE USING 5%, 10%, AND 20% MASKING RATIOS ON THREE DATASETS. THE MODEL WITH THE HIGHEST AUC IN EACH SETUP IS HIGHLIGHTED IN BOLD.

	eICU (AUC)			MIMIC_59 (AUC)			PhysioNet (AUC)		
	5%	10%	20%	5%	10%	20%	5%	10%	20%
V-RIN	0.88766 ± 0.012	0.88422 ± 0.013	0.88461 ± 0.015	0.83280 ± 0.010	0.83312 ± 0.012	0.82733 ± 0.014	0.83433 ± 0.011	0.82916 ± 0.010	0.82548 ± 0.015
BRITS	0.88669 ± 0.011	0.88521 ± 0.013	0.88569 ± 0.012	0.82821 ± 0.010	0.82779 ± 0.012	0.82414 ± 0.013	0.82214 ± 0.014	0.81175 ± 0.012	0.82181 ± 0.015
BRITS_GRU	0.88944 ± 0.012	0.88864 ± 0.015	0.88605 ± 0.011	0.83188 ± 0.010	0.83074 ± 0.012	0.82688 ± 0.013	0.80677 ± 0.014	0.81926 ± 0.013	0.80651 ± 0.015
GRUD	0.86495 ± 0.013	0.86456 ± 0.014	0.85801 ± 0.011	0.82768 ± 0.012	0.82640 ± 0.014	0.82304 ± 0.012	0.78997 ± 0.011	0.77652 ± 0.013	0.76989 ± 0.015
MRNN	0.87786 ± 0.011	0.87626 ± 0.014	0.87342 ± 0.015	0.82106 ± 0.012	0.81708 ± 0.011	0.81282 ± 0.013	0.80121 ± 0.014	0.79945 ± 0.013	0.79400 ± 0.015
CSAI	0.88952 ± 0.012	0.88977 ± 0.011	0.88795 ± 0.015	0.83524 ± 0.014	0.83367 ± 0.013	0.83109 ± 0.012	0.86465 ± 0.014	0.85919 ± 0.013	0.83722 ± 0.015

TABLE IV

CLASSIFICATION PERFORMANCE ON THE PHYSIONET DATASET USING 10% MASKING RATIO. THE IMPUTATION WAS PERFORMED USING THE PYPOTS IMPLEMENTATION OF THE MAJOR TRANSFORMER, RNN, CNN, GNN, DIFFUSION, AND STATISTICAL MODELS. FOR COMPARISON, IMPUTATION USING XGBOOST'S INTERNAL IMPUTER RESULTED IN ROC_AUC 0.771 ± 0.000

Model Type	Model	XGB Classifier	RNN Classifier	Transformer Classifier
Transformers	iTransformer	0.852 ± 0.000	0.692 ± 0.073	0.685 ± 0.032
	SAITS	0.851 ± 0.000	0.658 ± 0.076	0.668 ± 0.037
	ETSformer	0.820 ± 0.000	0.734 ± 0.030	0.678 ± 0.013
	PatchTST	0.848 ± 0.000	0.703 ± 0.064	0.698 ± 0.061
	Crossformer	0.836 ± 0.000	0.683 ± 0.051	0.644 ± 0.026
	Informer	0.836 ± 0.000	0.701 ± 0.021	0.653 ± 0.029
	Autoformer	0.768 ± 0.000	0.597 ± 0.009	0.625 ± 0.008
	Pyraformer	0.829 ± 0.000	0.739 ± 0.026	0.654 ± 0.047
Transformer	0.833 ± 0.000	0.723 ± 0.036	0.626 ± 0.036	
RNN	BRITS	0.841 ± 0.000	0.667 ± 0.066	0.646 ± 0.074
	MRNN	0.760 ± 0.000	0.611 ± 0.008	0.619 ± 0.015
	GRUD	0.840 ± 0.000	0.701 ± 0.075	0.704 ± 0.035
	CSAI	0.860 ± 0.000	0.702 ± 0.044	0.704 ± 0.023
CNN	TimesNet	0.823 ± 0.000	0.687 ± 0.087	0.710 ± 0.043
	MICN	0.824 ± 0.000	0.700 ± 0.071	0.686 ± 0.050
	SCIINet	0.818 ± 0.000	0.663 ± 0.055	0.720 ± 0.034
GNNs	StemGNN	0.809 ± 0.000	0.534 ± 0.124	0.701 ± 0.025
	FreTS	0.840 ± 0.000	0.693 ± 0.035	0.674 ± 0.018
	Koopa	0.835 ± 0.000	0.509 ± 0.113	0.628 ± 0.036
	DLinear	0.851 ± 0.000	0.689 ± 0.038	0.611 ± 0.053
	FiLM	0.825 ± 0.000	0.565 ± 0.095	0.706 ± 0.046
Diffus.	CSDI	0.853 ± 0.000	0.553 ± 0.108	0.762 ± 0.019
	US-GAN	0.839 ± 0.000	0.708 ± 0.019	0.610 ± 0.043
	GP-VAE	0.816 ± 0.000	0.745 ± 0.056	0.701 ± 0.041
Stats	Mean	0.763 ± 0.000	0.620 ± 0.017	0.598 ± 0.025
	Median	0.772 ± 0.010	0.619 ± 0.013	0.605 ± 0.025
	LOCF	0.795 ± 0.033	0.634 ± 0.074	0.644 ± 0.061
	Linear	0.807 ± 0.036	0.640 ± 0.076	0.669 ± 0.069

TABLE V

PERFORMANCE COMPARISON OF APPLYING OUR NON-UNIFORM MASKING STRATEGY ON DIFFERENT COMBINATIONS OF THE DATASET: TRAINING, VALIDATION AND TESTING. UNDER THE 'ALL' CONFIGURATION, NON-UNIFORM MASKING IS APPLIED DURING TRAINING, VALIDATION, AND TESTING CONSISTENTLY REPORTS THE PERFORMANCE (BOLD FONT).

Model	Masking	Imputation		Classification		
		Epoch	MAE	Epoch	MAE	AUC
BRITS	All	182.2	0.234929	28.6	0.262997	0.819142*
	Val_Test	187	0.235739	57	0.262268	0.816184
	Test_only	218.6	0.236001	61.6	0.265496	0.813821
	Train_only	215.8	0.266307	25.4	0.310624	0.815686
	None	218.6	0.26762	61.6	0.313257	0.81175
	Val_only	187	0.268386	57	0.309332	0.818605
BRITS-GRU	All	294.8	0.231594	21.8	0.26615	0.821869*
	Val_Test	287.4	0.233243	21.6	0.267872	0.813855
	Test_only	286	0.23363	15.4	0.270678	0.811355
	Train_only	288.4	0.258989	17.6	0.313681	0.815697
	Val_only	287.4	0.262149	21.6	0.314871	0.81071
	None	286	0.262155	15.4	0.318493	0.819258

representation of features is crucial for accuracy. However, for classification, increasing the weighting parameter leads to higher errors and a marginal decrease in the AUC, highlighting that excessive weighting may not uniformly improve performance across different machine learning tasks. These findings reveal the interplay between feature representation adjustments and task-specific model efficacy, underscoring the importance of calibration in the non-uniform masking approach for complex time series data.

TABLE VI

IMPACT OF WEIGHTING PARAMETER I ON IMPUTATION AND CLASSIFICATION PERFORMANCE METRICS. THE TABLE SHOWCASES THE NUMBER OF EPOCHS REQUIRED, IMPUTATION MAE AND CLASSIFICATION AUC ACROSS VARYING WEIGHTING FACTORS.

I	Imputation			Classification		
	Epoch	MAE		Epoch	MAE	AUC
0	286	0.26215514		15.4	0.31849296	0.8192579
5	291.2	0.2310647		33.8	0.26586726	0.80975966
10	294.8	0.23159396		21.8	0.26615049	0.8118691
50	293	0.24170042		16.4	0.28670924	0.81583396
100	285.8	0.26885496		14.2	0.32437366	0.81381879
150	283.8	0.29943347		16.6	0.35346112	0.8144707
200	289.2	0.33235399		15.6	0.39360851	0.81173828

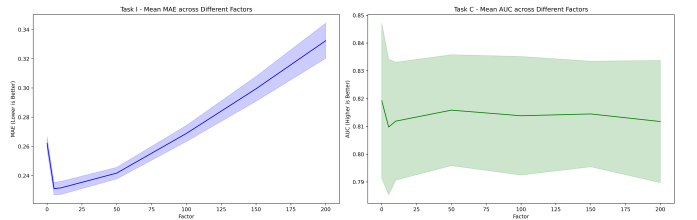


Fig. 5. Impact of Adjustment Factor on Model Performance in the Physionet Dataset.

VI. DISCUSSION AND CONCLUSIONS

This study introduced CSAI, a novel approach for imputing and classifying missing data in multivariate medical time series. CSAI's novelty lies in the provision of components specifically tailored to medical time-series, where the frequency and timing of data collection is highly variant, and long- and short-term correlations are pervasive. CSAI demonstrated significant potential to improve the accuracy and reliability of medical data analysis, which is critical for high-stakes

healthcare decision making. Using conditional knowledge embedding and attention mechanisms, CSAI outperformed established benchmarks in multiple real-world healthcare datasets, particularly in scenarios with lower masking ratios. Its ability to model non-random missingness and capture complex temporal relationships positions it as a valuable tool for the clinical domain.

Our comprehensive experimental evaluation showcased the efficacy of CSAI in diverse healthcare datasets, where it frequently surpassed baseline state-of-the-art models such as BRITS, BRITS-GRU, and others. CSAI consistently achieved the lowest imputation error and competitive classification performance in various masking configurations. The strong results suggest that CSAI can be instrumental in providing a strong base for predictive models used in various downstream tasks, including diagnosis and outcome prediction.

Future research on the interpretability of the CSAI imputation process could further enhance its applicability in clinical applications. Furthermore, the open-source nature of CSAI encourages ongoing collaboration and iterative improvements from the research community, which is crucial to advance the field and ensure its broader adoption in medical data analysis.

Future work should also explore incorporating more granular medical knowledge, improving the model’s ability to capture long-range temporal dependencies, and developing new methods for handling extreme data sparsity. Addressing these challenges could help CSAI achieve even better performance in various healthcare datasets with distinct characteristics and missing data patterns.

The potential applications of CSAI in medical data analysis and decision making are numerous. CSAI could enhance early detection of critical conditions like sepsis and cardiac arrest by providing more accurate imputations of incomplete patient records in real time. In addition, it could help improve prediction and treatment recommendations by effectively handling missing data from various data sources from patients. As CSAI continues to evolve, it holds promise of significantly contributing to more accurate and data-driven medical decision making and improved patient outcomes.

VII. ACKNOWLEDGMENTS

This paper represents independent research funded by the NIHR Maudsley Biomedical Research Centre at South London and Maudsley NHS Foundation Trust, the EPSRC Centre for Doctoral Training in Data-Driven Health (DRIVE-Health) and King’s College London. The work of LQ is supported by the Kings-China Scholarship Council PhD Scholarship Programme (K-CSC) under Grant CSC202008060096. ZI is supported by Innovate UK under grant 10104845. TW is supported by the NIHR Maudsley Biomedical Research Centre at South London, Maudsley Charity and Early Career Research Award from the Institute of Psychiatry, Psychology & Neuroscience. ZI and RD were supported by in part by the NIHR Biomedical Research Centre at SLaM, in part by Kings College London, London, U.K., and in part by the NIHR University College London Hospitals Biomedical Research Centre. H.L.E is supported by a Research Fellowship Award

from the Department of Medicine at Dalhousie University and DRIVE-Health. All experiments are implemented on CREATE HPC (King’s College London. (2022). King’s Computational Research, Engineering and Technology Environment (CRE-ATE)).

VIII. AVAILABILITY

CSAI is an open-source model. All code and experimental details are available on the CSAI GitHub repository <https://github.com/LinglongQian/CSAI>. CSAI is integrated into the PyPOTS ecosystem <https://docs.pypots.com/en/latest/pypots.imputation.html#module-pypots.imputation.csai> and is immediately callable from the Python package.

REFERENCES

- [1] J. R. et al, “Deep learning for electronic health records: A comparative review of multiple deep neural architectures,” *Journal of Biomedical Informatics*, vol. 101, p. 103337, 2020.
- [2] Z. M. Ibrahim, D. Bean, T. Searle, L. Qian, H. Wu, A. Shek, Z. Kraljevic, J. Galloway, S. Norton, J. T. H. Teo, and R. J. Dobson, “A knowledge distillation ensemble framework for predicting short- and long-term hospitalization outcomes from electronic health records data,” *IEEE Journal of Biomedical and Health Informatics*, vol. 26, no. 1, pp. 423–435, 2022.
- [3] F. E. Shamout, T. Zhu, P. Sharma, P. J. Watkinson, and D. A. Clifton, “Deep interpretable early warning system for the detection of clinical deterioration,” *IEEE Journal of Biomedical and Health Informatics*, vol. 24, no. 2, pp. 437–446, 2020.
- [4] R. H. et al., “Relationship between blood pressure and incident chronic kidney disease in hypertensive patients,” *Clinical Journal of the American Society of Nephrologists*, vol. 6, no. 11, 2011.
- [5] B. J. Wells, K. M. Chagin, A. S. Nowacki, and M. W. Kattan, “Strategies for handling missing data in electronic health record derived data,” *Egems*, vol. 1, no. 3, 2013.
- [6] L. Qian, T. Wang, J. Wang, H. L. Ellis, R. Mitra, R. Dobson, and Z. Ibrahim, “How deep is your guess? a fresh perspective on deep learning for medical time-series imputation,” 2024. [Online]. Available: <https://arxiv.org/abs/2407.08442>
- [7] P. Yadav, M. Steinbach, V. Kumar, and G. Simon, “Mining electronic health records (ehrs) a survey,” *ACM Computing Surveys (CSUR)*, vol. 50, no. 6, pp. 1–40, 2018.
- [8] P. B. Jensen, L. J. Jensen, and S. Brunak, “Mining electronic health records: towards better research applications and clinical care,” *Nature Reviews Genetics*, vol. 13, no. 6, pp. 395–405, 2012.
- [9] T. E. et al., “A survey on missing data in machine learning,” *Journal of Big Data*, vol. 8, p. 140, 2021.
- [10] H. Zhen, M. Genevieve, A. Elliot, W. Yan, K. Mary, and S. Gyorg, “Strategies for handling missing clinical data for automated surgical site infection detection from the electronic health record,” *Journal of biomedical informatics*, vol. 68, pp. 112–120, 2017.
- [11] W. Du, J. Wang, L. Qian, Y. Yang, F. Liu, Z. Wang, Z. Ibrahim, H. Liu, Z. Zhao, Y. Zhou, W. Wang, K. Ding, Y. Liang, B. A. Prakash, and Q. Wen, “Tsi-bench: Benchmarking time series imputation,” 2024. [Online]. Available: <https://arxiv.org/abs/2406.12747>
- [12] L. Qian, Z. Ibrahim, W. Du, Y. Yang, and R. J. Dobson, “Unveiling the secrets: How masking strategies shape time series imputation,” 2024. [Online]. Available: <https://arxiv.org/abs/2405.17508>
- [13] Z. Che, S. Purushotham, K. Cho, D. Sontag, and Y. Liu, “Recurrent neural networks for multivariate time series with missing values,” *Scientific reports*, vol. 8, no. 1, pp. 1–12, 2018.
- [14] W. Cao, D. Wang, J. Li, H. Zhou, L. Li, and Y. Li, “Brits: Bidirectional recurrent imputation for time series,” *Advances in neural information processing systems*, vol. 31, 2018.
- [15] J. Yoon, W. R. Zame, and M. van der Schaar, “Multi-directional recurrent neural networks: A novel method for estimating missing data,” in *Time series workshop in international conference on machine learning*, 2017.
- [16] J. Wang, W. Du, W. Cao, K. Zhang, W. Wang, Y. Liang, and Q. Wen, “Deep learning for multivariate time series imputation: A survey,” *arXiv preprint arXiv:2402.04059*, 2024.

- [17] C. Fang and C. Wang, "Time series data imputation: A survey on deep learning approaches," *arXiv preprint arXiv:2011.11347*, 2020.
- [18] Z. S. et al, "Self-supervised learning of time series representation via diffusion process and imputation-interpolation-forecasting mask," in *The 30th ACM SIGKDD Conference on Knowledge Discovery and Data Mining*, 2024, p. 2560–2571.
- [19] Q. Wen, T. Zhou, C. Zhang, W. Chen, Z. Ma, J. Yan, and L. Sun, "Transformers in time series: a survey," in *Proceedings of the Thirty-Second International Joint Conference on Artificial Intelligence*, ser. IJCAI '23, 2023.
- [20] W. Du, D. Côté, and Y. Liu, "Saits: Self-attention-based imputation for time series," *Expert Systems with Applications*, vol. 219, p. 119619, 2023.
- [21] S. Shan, Y. Li, and J. B. Oliva, "Nrtsi: Non-recurrent time series imputation," in *ICASSP 2023 - 2023 IEEE International Conference on Acoustics, Speech and Signal Processing (ICASSP)*, 2023, pp. 1–5.
- [22] E. Jun, A. W. Mulyadi, J. Choi, and H.-I. Suk, "Uncertainty-gated stochastic sequential model for ehr mortality prediction," *IEEE Transactions on Neural Networks and Learning Systems*, vol. 32, no. 9, pp. 4052–4062, 2020.
- [23] A. W. Mulyadi, E. Jun, and H.-I. Suk, "Uncertainty-aware variational-recurrent imputation network for clinical time series," *IEEE Transactions on Cybernetics*, 2021.
- [24] Y. Luo, X. Cai, Y. Zhang, J. Xu *et al.*, "Multivariate time series imputation with generative adversarial networks," *Advances in neural information processing systems*, vol. 31, 2018.
- [25] Y. Tashiro, J. Song, Y. Song, and S. Ermon, "Csdi: Conditional score-based diffusion models for probabilistic time series imputation," *Advances in Neural Information Processing Systems*, vol. 34, pp. 24 804–24 816, 2021.
- [26] L. Mescheder, A. Geiger, and S. Nowozin, "Which training methods for gans do actually converge?" in *International conference on machine learning*. PMLR, 2018, pp. 3481–3490.
- [27] T. e. a. Pollard, "The eicu collaborative research database, a freely available multi-center database for critical care research," *Scientific data*, vol. 5, no. 1, pp. 1–13, 2018.
- [28] S. Sheikhalishahi, V. Balaraman, and V. Osmani, "Benchmarking machine learning models on multi-centre eicu critical care dataset," *Plos one*, vol. 15, no. 7, p. e0235424, 2020.
- [29] A. Johnson and et al., "Mimic-iii, a freely accessible critical care database," *Scientific data*, vol. 3, no. 1, pp. 1–9, 2016.
- [30] H. Harutyunyan, H. Khachatrian, D. C. Kale, G. Ver Steeg, and A. Galstyan, "Multitask learning and benchmarking with clinical time series data," *Scientific data*, vol. 6, no. 1, p. 96, 2019.
- [31] I. Silva, G. Moody, D. Scott, L. Celi, and R. Mark, "Predicting in-hospital mortality of icu patients: The physionet/computing in cardiology challenge 2012," *Computational Cardiology*, vol. 39, p. 245–248, 2012.
- [32] W. Du, "PyPOTS: A Python Toolbox for Data Mining on Partially-Observed Time Series," 2023.
- [33] Y. Luo, Y. Zhang, X. Cai, and X. Yuan, "E2gan: End-to-end generative adversarial network for multivariate time series imputation," in *Proceedings of the 28th international joint conference on artificial intelligence*. AAAI Press Palo Alto, CA, USA, 2019, pp. 3094–3100.
- [34] R. Mitra, S. F. McGough, T. Chakraborti, C. Holmes, R. Copping, N. Hagenbuch, S. Biedermann, J. Noonan, B. Lehmann, A. Shenvi *et al.*, "Learning from data with structured missingness," *Nature Machine Intelligence*, vol. 5, no. 1, pp. 13–23, 2023.
- [35] A. Cini, I. Marisca, and C. Alippi, "Filling the `g_ap_s`: Multivariate time series imputation by graph neural networks," in *ICLR*, 2022. [Online]. Available: <https://openreview.net/forum?id=kOu3-S3wJ7>
- [36] M. Khayati, A. Lerner, Z. Tymchenko, and P. Cudré-Mauroux, "Mind the gap: an experimental evaluation of imputation of missing values techniques in time series," *Proc. VLDB Endow.*, vol. 13, no. 5, p. 768–782, Jan. 2020.